Reliability of EUCLIDIAN: An autonomous robotic system for image-guided prostate brachytherapy

Tarun K. Podder,[a] Ivan Buzurovic, Ke Huang, Timothy Showalter, Adam P. Dicker, and Yan Yu
Department of Radiation Oncology, Kimmel Cancer Center (NCI-designated), Thomas Jefferson University, Philadelphia, Pennsylvania 19107

(Received 13 January 2010; revised 5 November 2010; accepted for publication 9 November 2010; published 16 December 2010)

Purpose: Recently, several robotic systems have been developed to perform accurate and consistent image-guided brachytherapy. Before introducing a new device into clinical operations, it is important to assess the reliability and mean time before failure (MTBF) of the system. In this article, the authors present the preclinical evaluation and analysis of the reliability and MTBF of an autonomous robotic system, which is developed for prostate seed implantation.
Methods: The authors have considered three steps that are important in reliability growth analysis. These steps are: Identification and isolation of failures, classification of failures, and trend analysis. For any one-of-a-kind product, the reliability enhancement is accomplished through test-fix-test. The authors have used failure mode and effect analysis for collection and analysis of reliability data by identifying and categorizing the failure modes. Failures were classified according to severity. Failures that occurred during the operation of this robotic system were considered as nonhomogenous Poisson process. The failure occurrence trend was analyzed using Laplace test. For analyzing and predicting reliability growth, commonly used and widely accepted models, Duane's model and the Army Material Systems Analysis Activity, i.e., Crow's model, were applied. The MTBF was used as an important measure for assessing the system's reliability.
Results: During preclinical testing, 3196 seeds (in 53 test cases) were deposited autonomously by the robot and 14 critical failures were encountered. The majority of the failures occurred during the first few cases. The distribution of failures followed Duane's postulation as well as Crow's postulation of reliability growth. The Laplace test index was -3.82 (<0), indicating a significant trend in failure data, and the failure intervals lengthened gradually. The continuous increase in the failure occurrence interval suggested a trend toward improved reliability. The MTBF was 592 seeds, which implied that several prostate seed implantation cases would be possible without encountering any critical failure. The shape parameter for the MTBF was 0.3859 (<1), suggesting a positive reliability growth of this robotic system. At 95% confidence, the reliability for deposition of 65 seeds was more than 90%.
Conclusions: Analyses of failure mode strongly indicated a gradual improvement of reliability of this autonomous robotic system. High MTBF implied that several prostate seed implant cases would be possible without encountering any critical failure. [DOI: 10.1118/1.3523097]

Key words: brachytherapy robot, reliability of robot, medical robot, image-guided brachytherapy, prostate brachytherapy, prostate seed implant

I. INTRODUCTION

There has been considerable interest in the development of robotic systems for image-guided brachytherapy (IGBT), particularly for prostate seed implantation.[1–11] Major potential advantages of robotic assistance for IGBT include (1) improved accuracy, (2) increased consistency, and (3) reduction of clinician's fatigue. The majority of these robotic systems have been, for the most part, custom-made with in-house design and assembly. Although the various individual components that comprise these systems are tested for reliability and accuracy, it is important to evaluate the reliability of the entire system prior to introducing the device into use in clinical trials with human subjects. We have designed and developed a semiautomated robotic system, named Endo-Uro Computer Lattice for Intratumoral Delivery, Implantation, and Ablation with Nanosensing (EUCLIDIAN), which consists of a seven degrees-of-freedom (DOF) surgical module and a nine DOF positioning module.[4] Recently, we have completed rigorous preclinical trials that simulate the clinical procedures and permit evaluation of the system reliability.

The purpose of reliability growth analysis and testing is to enhance reliability over time through the modification and improvement in product design, development, manufacturing, and operating procedures. This paper presents the reli-

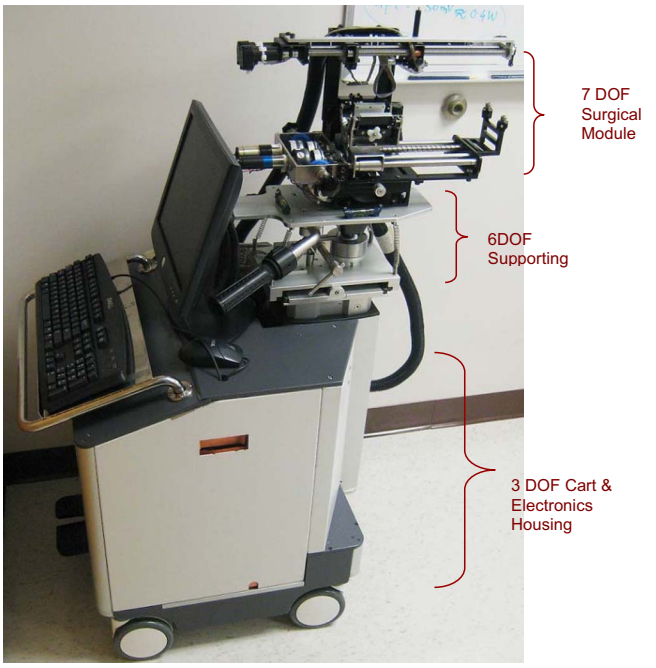

FIG. 1. EUCLIDIAN robot for brachytherapy.

ability growth analysis of the EUCLIDIAN robotic system during preclinical testing for seed delivery. This paper continues with a brief description of the system and reliability growth analysis using several different models, followed by the results and conclusions.

II. MATERIAL AND METHODS: SYSTEM OVERVIEW AND RELIABILITY ISSUES

The EUCLIDIAN (Fig. 1) is an ultrasound image-guided robotic system that is composed of several subsystems having a variety of different components. A majority of these components, such as motors, encoders, timing belts, pulleys, gears, clutches, shafts, lead screws, amplifiers, couplers, controllers, and so on, are commercially available and are designed independently. Most manufacturers can provide the mean time before failure (MTBF) rating for their component products. However, the MTBF of an entire robotic system cannot be considered to be the lowest common denominator of all of the subsystems or components because the functional interdependencies of subsystems and/or components reduce the reliability of the assembled/integrated system (R_{system}), which is the product of all the components' reliability $[R_{\text{system}}=(R_1\times R_2\times,\ldots,\times R_n)<\min(R_1,R_2,\ldots,R_n)$, since $R_i<1$; here, R denotes reliability]. The overall system reliability is a measure of the amount of time the robotic system as a whole has been operated properly, without any significant faults.[19,24] Significant or critical faults include those which may endanger patient safety and/or necessitate abandonment of the seed implant procedure. The three main modules that comprise the EUCLIDIAN are: (1) Surgical module, (2) positioning module, and (3) cart and electronic housing (Fig. 1). A very brief description of the EUCLIDIAN robot is as provided below.

II.A. Surgical module

The three main subsystems of the surgical module (Fig. 2) are: (1) Two DOF transrectal ultrasound (TRUS) probe driver (Figs. 1–3), (2) three DOF robotic gantry (Figs. 1 and 2), and (3) two DOF needle inserter with seed holder and seed pusher (Figs. 1, 2, and 4). A brief description of these subsystems is provided in the following sections.

II.A.1. Two DOF transrectal ultrasound probe driver

The TRUS probe, which contains two transducers (transverse and sagittal planes), can be translated and rotated separately by two motors fitted with high-resolution optical encoders (Fig. 3). This enables imaging the prostate in transverse as well as in sagittal planes with variable slice thicknesses or intervals (as thin as 0.1 mm). Working ranges of motion of the TRUS probe are 0–185 mm and −91° to +91° in translation and rotation, respectively. The TRUS probe can also be operated manually using the knobs; during

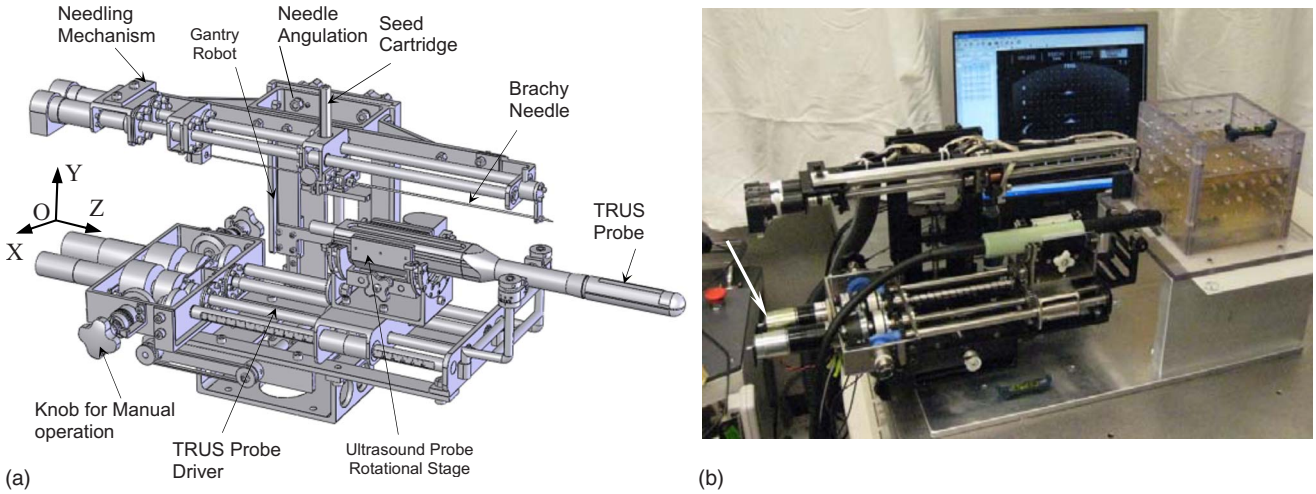

FIG. 2. Surgical module of EUCLIDIAN robot for brachytherapy.

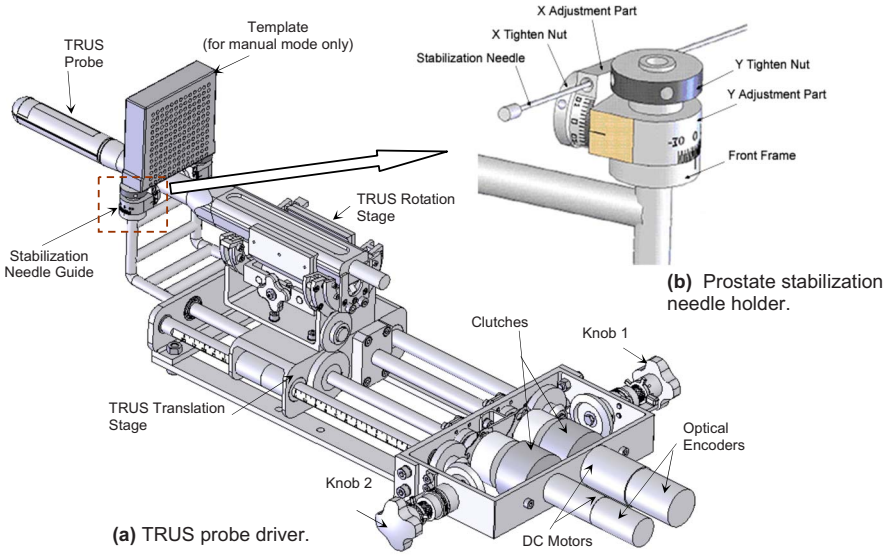

(a) TRUS probe driver.

(b) Prostate stabilization needle holder.

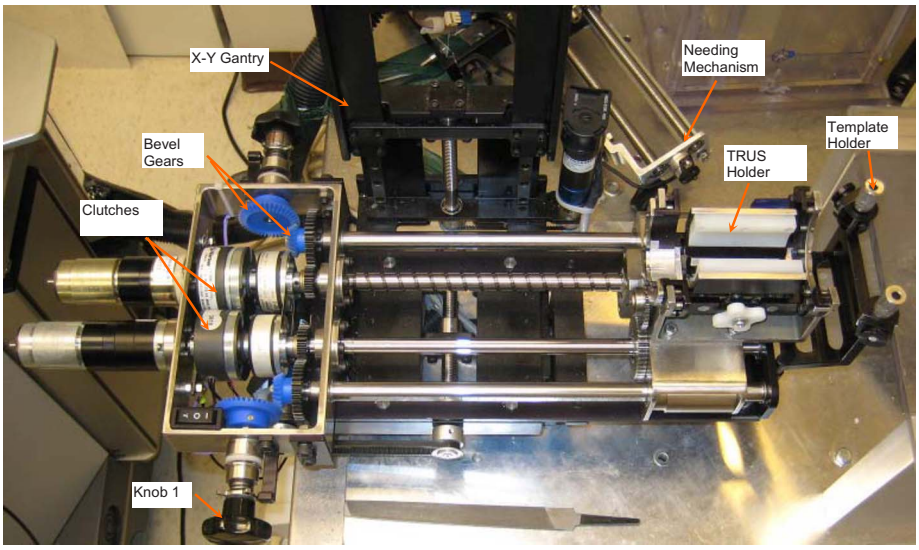

FIG. 3. TRUS probe driver and prostate stabilization needle holder of EUCLIDIAN robot.

this mode, the motors are disengaged automatically by electric clutches [Fig. 3(a)]. There is a provision for a template holder at the end of the TRUS probe driver (Fig. 3), enabling manual takeover if required. A pair of prostate stabilization needles can be placed with angulation in both sagittal and coronal planes to prevent the obstruction of robotic needle insertion. This approach has also been shown to produce significant improvement in prostate immobilization.[12]

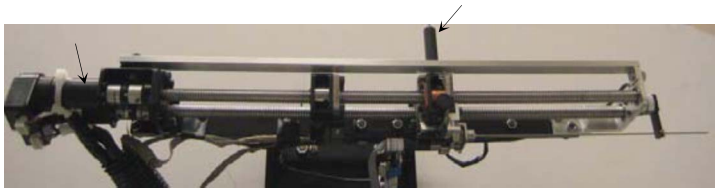

Fabricated needle driver and seed depositor.

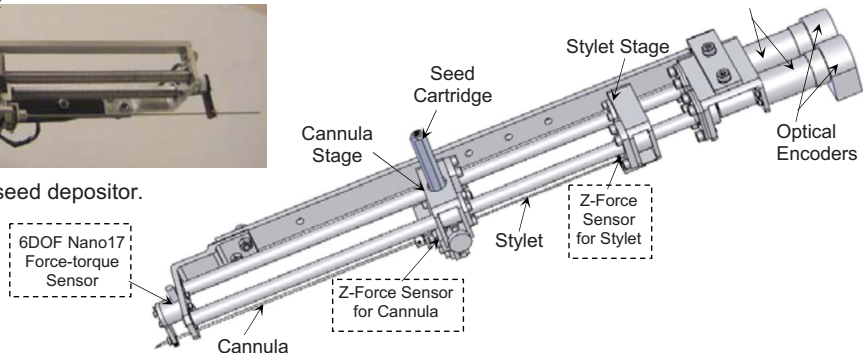

FIG. 4. Needle driver and seed depositor of EUCLIDIAN robot.

II.A.2. Three DOF robotic gantry

This subsystem, which features two translational motions (x- and y-direction) and one rotational motion (pitch, i.e., the rotation upward or downward about the x-axis), connects the needle driving module to the positioning platform. The motions are achieved by motors and optical encoders fitted with the motors (Figs. 1 and 2). The range of motion is 62 mm $\times$67 mm in the x-y direction. The rotational range for angulating the needle is $-5°$ to $+5°$ to avoid pubic arch interference and to reach the target region close to the TRUS probe. The TRUS probe motion and the rest of the surgery module (gantry and needle driver) are decoupled, as they are two separate open kinematic chains, which allow independent motions of the TRUS probe and the needle.

II.A.3. Two DOF needle inserter

The needle driver is the most complex subsystem of the EUCLIDIAN (Fig. 4), as the degree of complexity is increased with the introduction of three force-torque sensors (stylet sensor, cannula sensor, and whole needle sensor) cannula rotation and autonomous seed delivery system. The main components of this subsystem are: (1) Stylet driver, (2) cannula driver, (3) seed-cartridge holder, and (4) force-torque sensors. The cannula and the stylet are driven separately by two motors. The travel ranges of both the cannula and the stylet are 0–312 mm. During the surgical procedure, the motions of the cannula as well as of the stylet are autonomous in accordance with the treatment plan; however, the clinician must approve the movements at critical points. A detailed design and description of this subsystem is presented in a previous publication.[13] Our custom-designed seed cartridge can hold 35 seeds. Accommodation of additional seeds posed some challenges for smooth functioning of the seed cartridge due to spring nonlinearity. However, after careful investigation and adjustments, the seed cartridge is working satisfactorily. The *seed pusher*, a flat ended stylet, is deployed to expel the seed out of the cartridge and to deposit it at the planned location. Every motion during the sequence of seed delivery is fully automatic; however, the clinician is able to interrupt and/or manipulate the movements at any time using a hand pendant. By monitoring the force data from the sensor installed at the proximal end of the stylet (Fig. 4), the seed removal from the cartridge to the cannula can be verified.

II.A.4. Hand pendant

A ten-button hand pendant provides the clinician with the authority and freedom to assert control of the surgery module at any desired time. That is, the clinician can command each of the motors for manipulating the motion of various components of the surgical module, such as needle insertion, needle rotation, seed deposition, x-y movement of the gantry, and system abort.

In the case of system failure (if the motorized system totally fails), the EUCLIDIAN has a provision for conventional manual mode of operation. At the distal end of the TRUS probe driver, there is a holder for a conventional template; after inserting a regular commercial template, the clinician will be able to continue the seed implantation for the patient using the same dosimetric plan. Thus the patient treatment will not be affected if the clinician needs to switch to manual mode to perform a conventional prostate seed implant.

II.B. Positioning platform

The positioning platform has six DOF (translations along x-, y-, and z-axis and rotation about those axes), which allows translating and orienting the whole surgical module conveniently with respect to the patient's anatomical configuration (Fig. 1).

II.C. Cart and electronic housing

The three DOF cart (two translations and a rotation about the vertical axis) provides gross movement of the robotic system to align with the patient, while the six DOF platform enables finer movement for desired positioning and orientation of the robot in three-dimensional (3D) space. The computer, system electronics, and cable junctions are housed in the electronics housing (Fig. 1).

II.D. Electronics

The EUCLIDIAN's surgery module is fully autonomous; all the motors are fitted with high-resolution optical encoders and precision gear boxes. The robot is controlled by an industrial computer, which is proven to be robust and reliable for working in harsh industrial environments and military applications. It has a special metallic casing for minimizing electromagnetic interferences. This computer, equipped with Pentium 4 processor (2.8 GHz), 1 GB RAM, and eight PCI slots (Chassis Plans, San Diego, CA), is used for controlling the whole system. Two Galil control cards (Model DMC-1842; Galil Motion Control, Inc., Rocklin, CA) are used: One card to control the TRUS probe driver and gantry motions and the other card to control the needle driver and the seed pusher. A robust and stable proportional, integral and derivative (PID) controller has been developed for controlling the motorized surgical module. We have tuned the PID gains in such a manner so that the system's stability is maintained when the needle changes its states from merely position control in the air to both position and force control mode in the patient's body. The needle can be driven at a maximum velocity of approximately 100 mm/s; however, a lower velocity (60 mm/s) setting is used as the default.

A frame grabber (FlashBus, Integrated Technologies, Indianapolis, IN) is used for TRUS image capturing. Three force-torque sensors (Nano17, ATI Industrial Automation, Apex, NC and M13, Honeywell, Morristown, NJ) are used for needle insertion force monitoring and robot control feedback. Each of the motors is fitted with an optical encoder (MicroMo Electronics, Inc., Faulhaber Group, Clearwater, FL), which can provide final motion resolutions (considering gear ratios and screw leads) of 0.0007 mm for gantry x-y

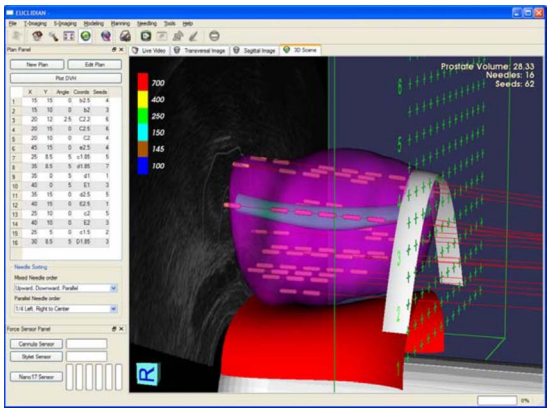

FIG. 5. Dosimetric planning with 2D display and 3D visualization.

translations, 0.004 mm for stylet and cannula motions, and 0.005 mm and 0.06° for TRUS probe translation and rotation, respectively.

II.E. Software and dosimetric plan

We have developed software in C++ with graphical user interface and drop-down menu (Fig. 5), which enables contouring, 3D anatomical model generation, dosimetric planning, 3D visualization, and needle tracking. The dosimetric plan is optimized using genetic algorithm based PIPER calculation engine at the core.[14] Isodose contours can be displayed on transverse, sagittal, and coronal planes of the prostate model built from TRUS images. In 3D visualization, various relevant anatomical structures, seeds, needle path, and virtual template along with the TRUS probe can be viewed (Fig. 5).

Further details of the EUCLIDIAN can be found in our previous publication.[4] While designing the electronics and deciding on what consumer off-the-shelf parts to use in the EUCLIDIAN robot, all parts were put through rigorous testing in the laboratory before final integration. The faults found in this testing phase were not included in this analysis since they were found prior to the system entering service and corrected at that time. Only faults that occurred after the integrated system was believed to be working correctly were logged and used later in reliability analysis.

II.F. Clinical workflow

A brief description of the clinical workflow is provided in this section along with a block diagram (Fig. 6). During the preclinical tests, we followed the clinical flow as closely as possible, except the first and the last steps (preliminary preparation and maintenance and storage; Fig. 6). For a real patient, in *setup state*, the EUCLIDIAN is initialized and patient information is entered into the computer by the user. Then, the TRUS is moved to scan the prostate in transversal

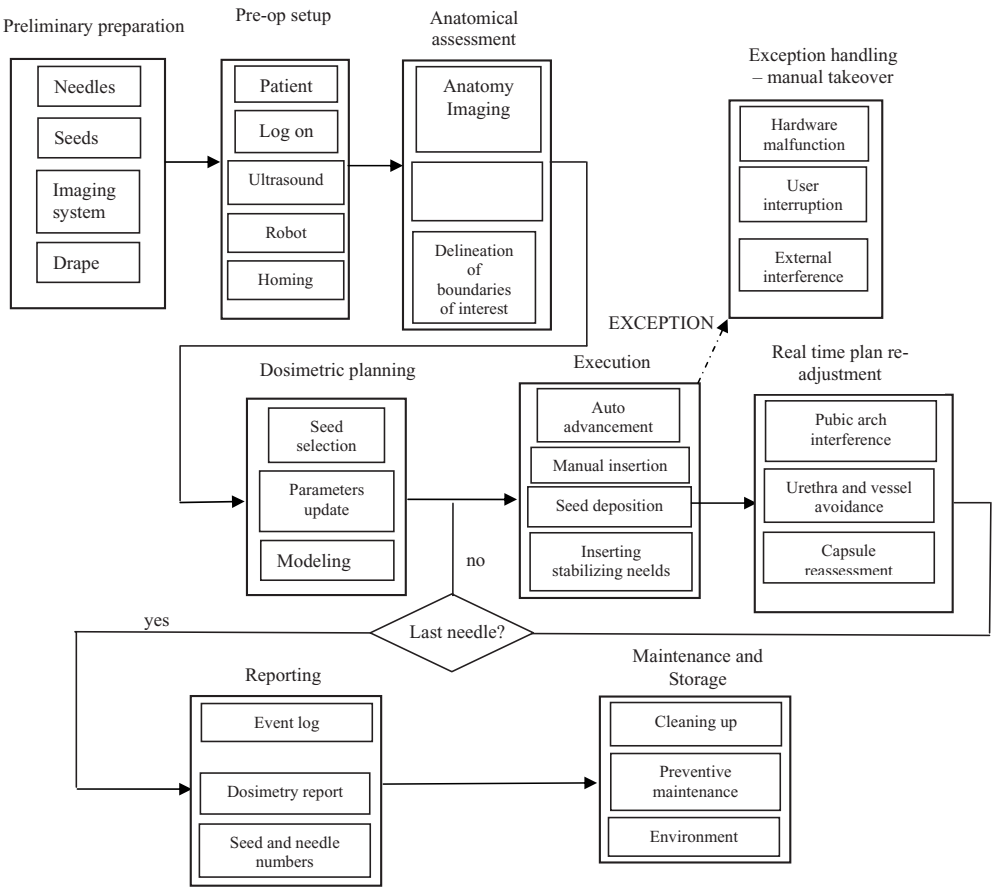

FIG. 6. Clinical workflow of a robot-assisted prostate brachytherapy using EUCLIDIAN.

plane and the images at a desired interval are saved. In the next step, the *modeling state*, the TRUS images are used in delineating the prostate, urethra, pubic bone, rectum, and seminal vesicle. Then, a 3D model of the prostate is generated automatically. This 3D model of the prostate is used for dosimetric planning to obtain the desired coordinates of the seed distribution. The software can display the planned isodose contours, needle position, and seed locations in 3D (Fig. 5). This provides the clinicians with a useful visualization of the whole treatment plan and, if required, the clinicians can edit the plan.

Once the plan is approved by the clinicians, a single needle is inserted by the robot into the patient (or phantom for preclinical tests) according to the plan. At this stage, the TRUS is employed in sagittal plane to tract the needle location. To ensure patient's safety, this needle insertion is performed in a sequential order. First, the *gantry robot* moves in the x-y direction to bring the tip of the needle close to the perineum of the patient and then the gantry is stopped. In the next step, the *needling mechanism* pushes the needle (stylet and cannula together) in to the patient/phantom to a predefined depth (about 10 mm away from the bladder). Then, the clinician uses the *hand pendant* to insert the needle to the final depth for seed placement. The clinician's manual adjustment using the hand pendant is to ensure patient safety, as well as to accommodate any change in planned depth that may be required due to tissue/organ deformation or needle deflection. After the needle insertion is completed, the system goes to the *implanting state*. In next step, the stylet pushes the seed from the cartridge and implants the seeds one by one according to the dosimetric plan. After completing the planned implant in a needle, the needle is fully withdrawn by the robot. As seeds are being delivered, the user may request the system go to the *validation state* to evaluate the latest dosimetry or skip the validation state and return to the *needling state*.

III. MATERIAL AND METHODS: RELIABILITY GROWTH ANALYSIS

For any one-of-a-kind product like the EUCLIDIAN, reliability enhancement is accomplished through iterative, test-fix-test cycles of the product evaluation and adjustment process.[19] The failure mode and effect analysis (FMEA) was used for collection and analysis of reliability data by identifying and categorizing the failure modes. Failures were classified according to severity. Discussion on FMEA can be found in various publications;[15–19] interested readers are encouraged to consult the text book in reference.[19] Failures that occurred in EUCLIDIAN operations were considered as nonhomogeneous Poisson process (NHPP)[15–17] and the trend was analyzed using Laplace test.[18,19] For analyzing and predicting reliability growth, commonly used and widely accepted models, Duane's model and Crow's model, were applied. The MTBF was used as an important measure for assessing reliability of the system.

This work focuses on the reliability growth analysis and testing as an endeavor to enhance reliability over time through modification and improvement in product design, development, manufacturing, and operating procedures. In a test-fix-test strategy for iterative evaluation of a device, failure modes are found during the testing and corrective actions for these problems are incorporated during the test. After each significant failure, corrective actions were taken and then the EUCLIDIAN was deployed for next test. Additionally, for any one-of-a-kind product, FMEA is essential for collecting and analyzing the reliability data by identifying and categorizing failure modes. Actions taken during growth testing include the correction of design weaknesses and manufacturing flaws and the elimination of inferior parts or components. Therefore, the steps important in reliability growth analysis are: (1) Identification and isolation of failures, (2) classification of failures (or severity analysis), and (3) trend analysis.[20,21]

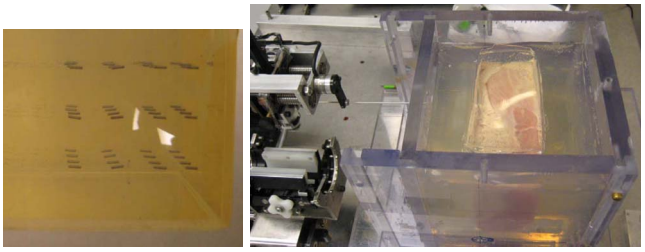
(a) (b)

FIG. 7. Seeds deposition—Experimental setup.

The preclinical experimental setup is shown in Fig. 7. We used two types of phantoms:[22] (1) Plastisol gel [polyvinylchloride; Fig. 7(a)], a combination of supersoft plastic and softener or hardener (MF Manufacturing Co., Fort Worth, TX) and (2) soft animal tissue (chicken breast) phantom [Fig. 7(b)]. The phantom materials are put into a Plexiglas box about 15 cm × 15 cm × 13 cm, which has provision for TRUS probe insertion through a long cylindrical opening at the bottom mimicking the rectum. Dummy seeds were deposited according to the dosimetric plans and clinical workflow mentioned in Sec. II F.

III.A. Identification and isolation of failures

In the past 6 months, EUCLIDIAN was tested rigorously in the preclinical setting. During this time the robotic system encountered several different types of failures. It was very important to identify these early failures when they occurred, so that appropriate actions could be taken. In practice, we always observe the effects, but may not be able to determine the causes immediately. Sometimes it is difficult, if not impossible, to identify and isolate the faults and their causes. However, we were able to identify and isolate all the failures of the EUCLIDIAN. A descriptive list of the 14 failures observed during 53 tests of the EUCLIDIAN is provided in Table I.

III.B. Classification of failures

The failures that generally occur during any robotic system operation can be categorized in several ways based on:

TABLE I. List of failures that occurred during EUCLIDIAN operation. Note: Severity of failures: A=no/minimum action taken; B=action taken; BB1=extremely critical; BB2=moderately critical; BB3=not critical.

Cumulative failure no.	Test no.	Failure mode (cause/action)	Cumulative no. of seeds	Severity of failure
1	1	At the beginning, two seeds delivered together (force-feedback antistuck strategy; mechanism adjusted)	1	B (BB1)
2	2	After five seed delivery, two seeds delivered together (force-feedback antistuck strategy; mechanism readjusted)	42	B (BB1)
3	3	At the beginning, two seeds delivered together (force-feedback antistuck strategy; mechanism readjusted)	72	B (BB1)
4	3	After two seed delivery, three seeds delivered together (force-feedback antistuck strategy; mechanism modified)	75	B (BB1)
5	4	No delivery—Stylet stuck (misalignment; adjusted the alignment)	108	B (BB2)
6	6	Last two seeds remained in the cartridge (spring was too loose; adjusted spring force)	214	B (BB3)
7	11	Seed implanter failure reported (mechanical misalignment; adjusted the alignment)	215	B (BB2)
8	12	Seed stuck (cartridge misalignment; adjusted the alignment)	446	B (BB2)
9	14	Seed stuck (seed misalignment in cartridge; seed pushed out manually)	509	B (BB2)
10	17	Seed Implanter failure reported (angulated needle issue)	571	B (BB2)
11	23	Seed stuck (seed misalignment in cartridge; seed pushed out manually)	1276	B (BB2)
12	27	Seed stuck (seed misalignment in cartridge; seed pushed out manually)	1629	B(BB2)
13	37	Seed stuck (seed misalignment in cartridge; seed pushed out manually)	2273	B(BB2)
14	50	Seed stuck (seed misalignment in cartridge; seed pushed out manually)	2949	B(BB2)

(1) *Subsystem* (which subsystem or component failed), (2) *function (*which function or workability has been jeopardized because of the failure), and (3) *severity* (what is the effect/impact of the failure on the assigned mission). Here we classify the failures according to the severity, i.e., effect or impact of the failure on the accomplishment of the seed implant procedures. The failures and their classification are presented in Table I.

Here, critical or major failures were those for which the seed deposition process was stopped and the robot had to be restarted after resolving the issue. We observed, on an average, less than one minor fault per test. These minor faults were mainly due to human errors, such as forgetting to put the seed cartridge (because of overlooking the warning/error message), did not tighten the seed plunder adequately, did not tighten the set screws on the needle adequately, and obstructing robotic motion by putting undesired objects. For reducing human errors, the users are strongly recommended to read the EUCLIDIAN's user manual.[29] Minor faults, which were detected and rectified on the fly without disturbing the seed deposition process, have not been included in Table I. It was observed that a majority of failures (11 of 14) originated from within the seed cartridge. Note that the needle insertion and seed deposition tasks are performed autonomously, not manually. This is quite challenging. One of the critical issues in identification and isolation, as well as classification of failures, is the documentation of the failure modes and its effects. Sometimes it may be difficult, if not impossible, to interpret the failure history due to poor or misleading information or documentation. Therefore, it is important to document the failures immediately or at the earliest convenience. All of these issues make the analysis of reliability more difficult. A better practice would be to document the failure in the FMEA chart immediately.

III.C. Trend analysis

In case of any one-of-a-kind product like the EUCLIDIAN, it is important to determine the failure trend, i.e., whether the failure rate is increasing or decreasing with the time of operation. Failures occurring in the EUCLIDIAN operations can be considered as *stochastic point processes*. In this type of NHPP, the point process is nonstationary, such that the distribution of the number of events in an interval of fixed length changes as the number of events increases. Therefore, the trend can be analyzed using the statistics of *event series* such as centroid test or Laplace test, which states the test statistic for trend as follows:[18,19,23]

$$\xi = \frac{\Sigma t_i/N - T/2}{T\sqrt{1/(12N)}}, \tag{1}$$

where t_i is the arrival values of each event, i.e., time to failure, T is the period of observation (here, total number of seeds deposited), and N is the number of events, i.e., the failures. If the Laplace index $\xi=0$, there is no trend, i.e., the process is stationary. If $\xi<0$, the failure occurrence trend is decreasing, i.e., the failure occurrence interval values tend to become larger. Conversely, when $\xi>0$, the trend is increasing, i.e., interval values tend to become progressively smaller.

The most commonly used and widely accepted models for analyzing and predicting reliability growth of a system are: (1) Duane's model and (2) Crow's model or Army Material Systems Analysis Activity (AMSAA) model. These models are briefly described below.

III.C.1. Duane's model

Duane's model states that a plot of the cumulative number of failures per test time versus the test time during growth testing is approximately linear when both are plotted on a logarithmic scale.[25] This observation can be expressed mathematically and then extrapolated to predict the growth in MTBF.

III.C.2. Crow's model

This model attempts to track the reliability within a series of growth testing cycles. At the end of each design change cycle, the failure rates decrease and the behavior of the failure rates is approximated as a continuous curve of the form at^b, which leads to a linear relationship between the cumulative failure rate and the observation time when plotted on a log-log scale.[24,26,27] Although Crow's model (AMSAA model) has the same mathematical form as Duane's model, the AMSAA model is often applied to a single test phase/cycle, whereas Duane's model attempts to account for the global change in failure rates and MTBFs.[19]

In case of type I data, i.e., for a given N successive failure times $t_1<t_2<,\ldots,<t_N$ that occur prior to the accumulated test time or observed system time (here, number of seed deposited) T, the shape parameter β for the AMSAA model is written as follows:[15–19,25]

$$\beta = \frac{N}{N\ln T - \Sigma_{i=1}^{N}\ln t_i}. \tag{2}$$

A relatively simple model of a stochastic point process is the NHPP, in which the scale parameter, i.e., intensity function of power law process (also known as Weibull failure rate function) is

$$\lambda(T) = \alpha\beta T^{\beta-1}, \quad \alpha,\beta>0, \tag{3}$$

where the cumulative number of failure is $\alpha=N/T^{\beta}$. Although, Eq. (3) is more commonly found in literature, one can use a simpler form as follows:

$$\lambda(T) = N\beta T^{-1}. \tag{4}$$

The parameters α and β are generally estimated using least-square methods.[15–17] Then the MTBF is written as

$$\text{MTBF} = \frac{1}{\lambda(T)}. \tag{5}$$

Two-sided confidence intervals (CIs) for MTBF can be obtained from the following expression:

$$\frac{L}{\lambda(T)} \le \text{MTBF} \le \frac{U}{\lambda(T)}, \tag{6}$$

where L and U are the lower and upper confidence interval factors. This model is applicable for test-fix-test strategies of operations, where the problem modes are found during testing and corrective actions for these problems are incorporated during the test. For the EUCLIDIAN robot, the number of seed deposition, i.e., delivery, is considered equivalent to time parameter in the above expressions.

III.C.3. Reliability bounds

$$\text{If} \quad 0<\lambda_L \le \lambda(t) \le \lambda_U, \tag{7}$$

$$\text{Then} \quad \int_0^t \lambda_L dt' \le \int_0^t \lambda(t')dt' \le \int_0^t \lambda_U dt', \tag{8}$$

$$\text{and} \quad \exp\left[-\int_0^t \lambda_L dt'\right] \ge \exp\left[-\int_0^t \lambda(t')dt'\right] \ge \exp\left[-\int_0^t \lambda_U dt'\right], \tag{9}$$

$$\text{or} \quad e^{-\lambda_L t} \ge R(t) \ge e^{-\lambda_U t}. \tag{10}$$

Therefore, if the hazard rate function $\lambda(t)$ is bounded, the reliability function $R(t)$ can also be bounded. According to Barlow and Porschan[28] for a decreasing failure rate process, reliability is

$$R(t) = \begin{cases} e^{-t/\text{MTBF}} & \text{for} \quad t \le \text{MTBF} \\ \dfrac{\text{MTBF}}{t}e^{-1} & \text{for} \quad t > \text{MTBF} \end{cases}. \tag{11}$$

IV. RESULTS AND DISCUSSION

The distribution of the failures during seed deposition has been graphically presented in Fig. 8. It reveals that the best-fitting curve follows the power law ($R^2=0.94$) and the next best one is the logarithmic fitting ($R^2=0.84$). The distribution of failure is nonhomogeneous; however, we observe a decrease in failure occurrence as the seed deposition process continues. By substituting data from Tables I and II ($T=3196$ is the total number of seed deposited during the 53 test period considered) into Eq. (1), we obtain the Laplace index $\xi=-3.82\ll1$. This indicates two important points: (1) There is a significant trend in the EUCLIDIAN's failure data

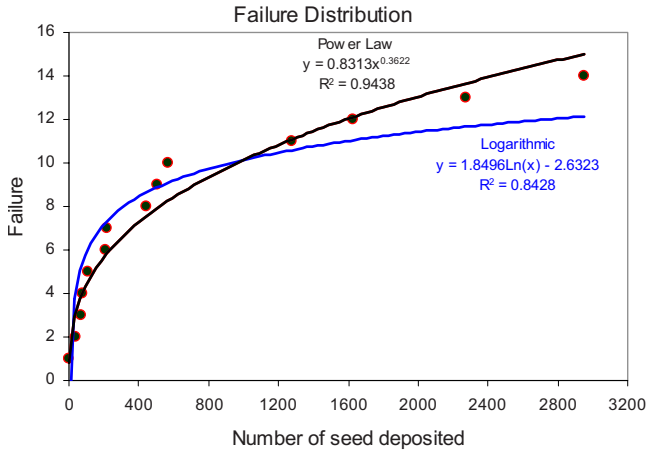

FIG. 8. Distribution of the failures during EUCLIDIAN's preclinical tests.

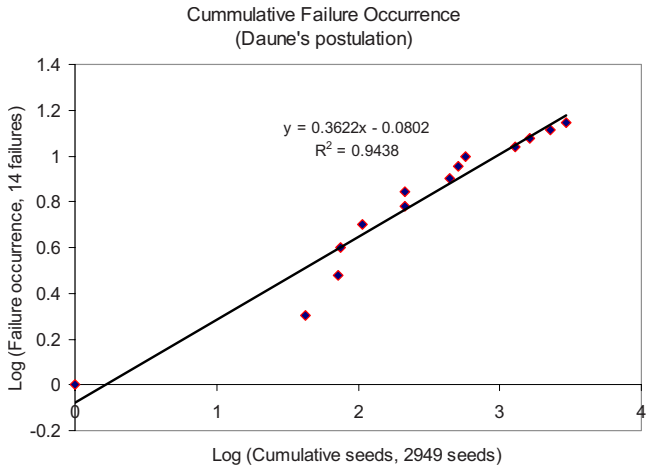

FIG. 9. Cumulative failure occurrence—Duane's postulation.

and (2) the failure occurrence intervals are gradually becoming larger. Since the failure occurrence interval is increasing, i.e., less number of failures in a particular time (seed deposition) interval, thus the system reliability exhibits an increasing trend.[28]

MTBF is an important measure for assessing reliability of a product in operation. We have computed the MTBF and other relevant parameters using Eqs. (2)–(6) of the AMSAA model (summary is provided in Table II). Taking values from Tables I and II, we obtained the shape parameter $\beta=0.3859$, Weibull failure rate function $\lambda=0.0017$, and the corresponding MTBF=592. It is to be noted that $\beta=1$ means no reliability growth, $\beta<1$ indicates positive reliability growth, and $\beta>1$ implies negative reliability growth. Here, $\beta=0.3859<1$, which indicates a positive reliability growth for the EUCLIDIAN. From the chi-square (χ^2) statistics for the trend test, we found $\chi^2=2N/\beta=72.6>\chi^2_{\text{crit},0.05}=38.9$. Therefore, the hypothesis of significant trend is accepted. Since β is much less than 1, the EUCLIDIAN's reliability is improving rapidly.

The lower limit and upper limit of the MTBF have been computed using Eq. (6) and values for confidence interval factors (L, U) from a standard data table. This data table is readily available in text books or handbooks on reliability.[19,20] The range of the MTBF is relatively large (Table II), which is expected to be narrowed with increased number of data set and decreased number of failures. The lower limit of the MTBF at 95% CI is 268, which is adequate for completing four to five prostate seed implant cases without encountering any critical failure. However, the nominal MTBF at 95% CI is 592, indicating more cases (maybe seven to ten cases) would be possible without facing any critical failures.

The log-log plot of cumulative failure versus cumulative time, in Fig. 9, conforms to Duane's postulation of linear relationship having a correlation coefficient of 0.94. The slope of this line is about 0.36 (>0), which is also an indication of change in failure occurrence; the rate of number of failures decreases as time increases. In Fig. 10, we have plotted cumulative failure rate versus cumulative time on a log-log scale. This plot clearly agrees with Crow's postulation of liner relationship. The negative slope of the failure curve indicates a significant trend in decreasing failure rates as the number of seed deposition increases. It is to be noted that Duane's model captures the global trend of failure rates, whereas Crow's model indicates the failure rates during a

TABLE II. Summary of the tests and results.

Total number of seeds deposited	3196
Total number of tests	53
No. of seeds deposited per test	
Range	29–81
Mean	60.3
Median	64
MTBF	(at 95% CI)
Nominal	592
Range	268–1597
Laplace index (ξ)	−3.82 (at 95% CI)
Shape parameter (β)	0.3859

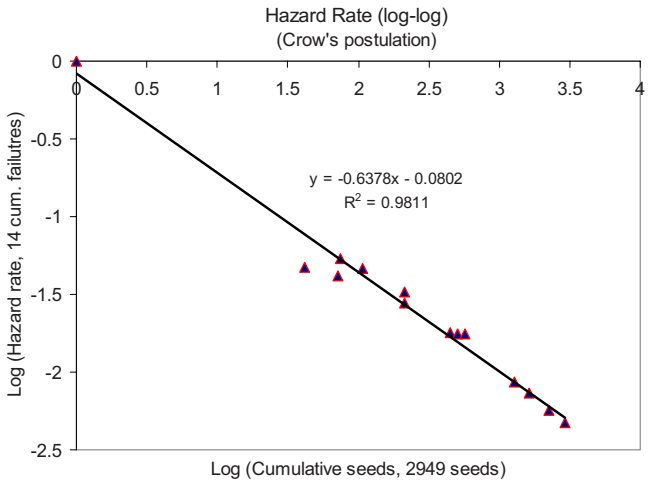

FIG. 10. Hazard rate—Crow's postulation.

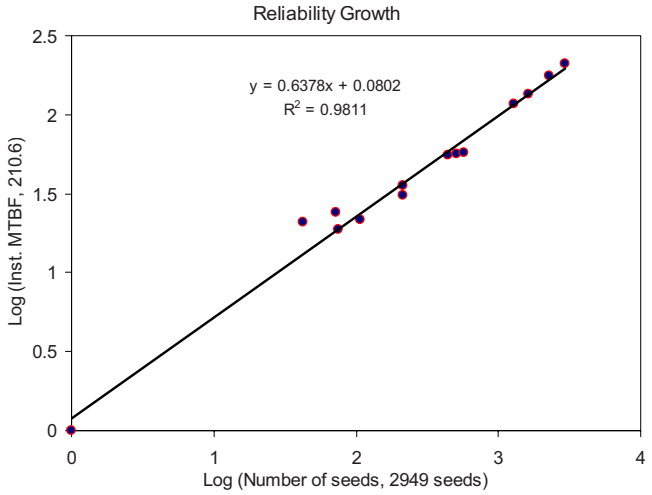

FIG. 11. Trend of reliability growth. The slope of this line (0.638 > 0) *is an indicator of reliability growth.*

single test phase. Conformation to both the Crow's and Duane's postulations indicates strong reliability growth of the EUCLIDIAN.

The cumulative MTBFs for 14 failures are presented in Fig. 11. It also exhibits linear relationship on a log-log plot. It is observed that the MTBF has improved with increased number of seed deposition. This indicates a growth in system's reliability as the process continues. The reliability bounds of the EUCLIDIAN robot for seed deposition operation have been presented in Fig. 12. The system reliability is quite impressive; for example, 65 seeds would be deposited with a reliability of 90% at 95% CI. For the same number of seeds, the reliability bound is 80%–96% at 95% CI. However, from the growing trend of the MTBF, we can expect significant improvement in the reliability in the future.

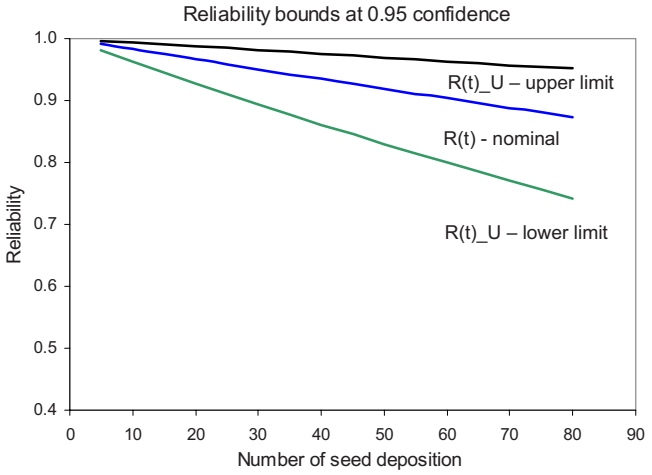

FIG. 12. Bounds of the reliability of EUCLIDIAN at 95% CI. R(t) is the nominal reliability, R(t)_U is the upper limit of reliability, and R(t)_L is lower limit of reliability.

V. CONCLUSION

The strategy that is commonly followed for testing one-of-a-kind type of products like the EUCLIDIAN is *test-fix-test*. During the preclinical testing phases of the EUCLIDIAN, we have collected all the failure data to analyze the reliability trend of the system. It has been observed that the MTBF is increasing, i.e., the system is becoming more reliable with time. This is plausible because when the system failure is analyzed at the subsystem or component level, the required component/subsystem is modified or replaced with an improved one.

The failure distribution closely follows Duane's postulation as well as Crow's postulation, which indicates reliability growth during the test phase as well as improved global trend. Both the Laplace test and the chi-square test revealed a significant positive trend in reliability growth. The nominal MTBF is 592, which means that several seed implant cases would be possible without encountering any critical failure. However, with the increasing reliability trend, it is expected that the consistency in the MTBF (range 268–1597 at 95% CI) and system reliability (0.80–0.96 for 65 seeds at 95% CI) would be improved, while more tests are performed and additional data are incorporated in the analysis. The EUCLIDIAN is currently in regular preclinical operations and undergoing occasional upgrades of both hardware and software. Generally, the majority of the failures encountered during the engineering development phase no longer occur. In the preclinical test operation phase, the robot has become more stable and reliable. It appears that the methodologies used in this study can be quite useful for evaluating reliability growth and/or reliability of any systems (especially newly introduced/developed) including robots for medical applications.

ACKNOWLEDGMENTS

This study is partly supported by the National Cancer Institute (NCI) Grant No. R01-CA091763, the NCI Grant No. P30-CA056036-09, and the Department of Defense Grant No. W81XWH-06-1-0227.

[a]Electronic mail: poddert@ecu.edu

[1]D. Stoianovici *et al.*, "AcuBot: A robot for radiological percutaneous interventions," IEEE Trans. Rob. Autom. **19**, 927–930 (2003).
[2]Z. Wei *et al.*, "Robot-assisted 3D-TRUS guided prostate brachytherapy: System integration and validation," Med. Phys. **31**, 539–548 (2004).
[3]G. Fichtinger *et al.*, "Robotically assisted prostate brachytherapy with transrectal ultrasound guidance—Phantom experiments," Brachytherapy **5**, 14–26 (2006).
[4]Y. Yu *et al.*, "Robotic system for prostate brachytherapy," J. Comp. Aid. Surg. **12**(6), 366–370 (2007).
[5]M. A. Meltsner, "Design and optimization of a brachytherapy robot," Ph.D. thesis, Department of Medical Physics, University of Wisconsin-Madison, 2007.
[6]M. A. Meltsner, N. J. Ferrier, and B. R. Thomadsen, "Observations on rotating needle insertions using a brachytherapy robot," Phys. Med. Biol. **52**, 6027–6037 (2007).
[7]D. Stoianovici *et al.*, "MRI stealth robot for prostate interventions," Minimally Invasive Therapy **16**(4), 241–248 (2007).
[8]T. K. Podder, W. S. Ng, and Y. Yu, "Multi-channel robotic system for prostate brachytherapy," in Proceedings of the International Conference of the IEEE Engineering in Medicine and Biology Society (EMBS), Lyon, France, pp. 1233–1236, 23–26 August 2007.

[9]S. E. Salcudean *et al.*, "A robotic needle guide for prostate brachytherapy," in Proceedings of the IEEE International Conference on Robotics and Automation (ICRA), Anaheim, CA, pp. 2975–2981, 19–23 May 2008.
[10]A. Lin, A. L. Trejos, R. V. Patel, and R. A. Malthaner, "Robot-assisted minimally invasive brachytherapy for lung cancer," *Teletherapy* (Springer, Berlin, 2008), pp. 33–52.
[11]M. Moerland *et al.*, "An MRI scanner compatible implant robot for prostate brachytherapy," Brachytherapy **7**, 100–100 (2008).
[12]T. K. Podder *et al.*, "Methods for prostate stabilization during transperineal LDR brachytherapy," Phys. Med. Biol. **53**, 1563–1579 (2008).
[13]Y. D. Zhang *et al.*, "Design and experiments of seed delivery device for prostate brachytherapy," in Proceedings of the IEEE International Conference on Intelligent Robots and Systems (IROS), Beijing, China, pp. 1280–1284, 9–15 October 2006.
[14]E. M. Messing *et al.*, "Intraoperative optimized inverse planning for prostate brachytherapy: Early experience," Int. J. Radiat. Oncol., Biol., Phys. **44**, 801–808 (1999).
[15]H. Ascher and H. Feingold, *Repairable Systems Reliability* (Dekker, New York, 1984).
[16]M. J. Crowder *et al.*, *Statistical Analysis of Reliability Data*, 1st ed. (Taylor & Francis, New York, 1991).
[17]J. F. Lawless, *Statistical Models and Methods for Lifetime Data* (Wiley, Hoboken, 2003).
[18]L. J. Brian and M. Engelhardt, *Statistical Analysis of Reliability and Life-Testing Models*, 2nd ed. (Dekker, New York, 1991).
[19]C. E. Ebeling, *An Introduction to Reliability and Maintainability Engineering*, 1st ed. (McGraw-Hill, New York, 1997).
[20]Department of Defense, *Military Handbook, Reliability Growth Management (MIL-HDBK-189)* (Naval Publications and Forms Center, Philadelphia, 1981).
[21]T. K. Podder, M. Sibenac, H. Thomas, R. Fuhrmann, and J. G. Bellingham, "Reliability growth for autonomous underwater vehicle—Dorado: An analysis of the experimental data," in Proceedings of the IEEE/MTS International Conference—OCEANS, Kobe, Japan, pp. 856–862, 9–12 November 2004.
[22]T. K. Podder, I. Buzurovic, K. Huang, A. P. Dicker, and Y. Yu, "Reliability growth of a fully automated robotic system," Med. Phys. **36**, 2424–2424 (2009).
[23]T. K. Podder, D. P. Clark, J. Sherman, D. Fuller, D. J. Rubens, W. S. Ng, E. M. Messing, J. G. Strang, Y. D. Zhang, and Y. Yu, "Robotic needle insertion in soft material phantoms: An evaluation of properties of commonly used soft materials," in Proceedings of the IEEE International Conference on Biomedical Engineering (ICBME), Singapore, 7–10 December 2005.
[24]P. D. T. O'Connor, *Practical Reliability Engineering*, 4th ed. (Wiley, Chichester, 2002).
[25]J. T. Duane, "Learning curve approach to reliability monitoring," IEEE Transactions on Aerospace **2**(2), 563–566 (1964).
[26]L. H. Crow, "Reliability analysis for complex repairable systems," in *Reliability and Biometry*, edited by F. Proschan and R. J. Serfing (SIAM, Philadelphia, 1974), pp. 379–410.
[27]L. H. Crow, "An extended reliability growth model for managing and assessing corrective action," in Proceedings of the IEEE Reliability and Maintainability Symposium, pp. 73–80, 2004.
[28]R. E. Barlow, F. Proschan, and L. C. Hunter, *Mathematical Theory of Reliability* (Wiley, New York, 1967).
[29]T. K. Podder, K. Yan, I. Buzurovic, and Y. Yu, User's Manual for EUCLIDIAN Robot (Department of Radiation Oncology, Thomas Jefferson University, Philadelphia, PA, 2007).